
LSMS: Language-guided Scale-aware MedSegmentor for Medical Image Referring Segmentation

Shuyi Ouyang
Zhejiang University

Jinyang Zhang
Zhejiang University

Xiangye Lin
Zhejiang University

Xilai Wang
Zhejiang University

Qingqing Chen
Sir Run Run Shaw Hospital

Yen-Wei Chen
Ritsumeikan University

Lanfen Lin
Zhejiang University

Abstract

Conventional medical image segmentation methods have been found inadequate in facilitating physicians with the identification of specific lesions for diagnosis and treatment. Given the utility of text as an instructional format, we introduce a novel task termed Medical Image Referring Segmentation (MIRS), which requires segmenting specified lesions in images based on the given language expressions. Due to the varying object scales in medical images, MIRS demands robust vision-language modeling and comprehensive multi-scale interaction for precise localization and segmentation under linguistic guidance. However, existing medical image segmentation methods fall short in meeting these demands, resulting in insufficient segmentation accuracy. In response, we propose an approach named Language-guided Scale-aware MedSegmentor (LSMS), incorporating two appealing designs: (1) a Scale-aware Vision-Language Attention module that leverages diverse convolutional kernels to acquire rich visual knowledge and interact closely with linguistic features, thereby enhancing lesion localization capability; (2) a Full-Scale Decoder that globally models multi-modal features across various scales, capturing complementary information between scales to accurately outline lesion boundaries. Addressing the lack of suitable datasets for MIRS, we constructed a vision-language medical dataset called Reference Hepatic Lesion Segmentation (RefHL-Seg). This dataset comprises 2,283 abdominal CT slices from 231 cases, with corresponding textual annotations and segmentation masks for various liver lesions in images. We validated the performance of LSMS for MIRS and conventional medical image segmentation tasks across various datasets. Our LSMS consistently outperforms on all datasets with lower computational costs. The code and datasets will be released.

1 Introduction

The significance of organ segmentation and lesion segmentation in medical image analysis has been widely recognized [29, 43]. As shown in Figure 1(a), the classical medical image segmentation task involves inputting a medical image and obtaining segmentation results encompassing all lesions within the image [3, 33]. With the advancement of multi-modal research, studies have emerged that incorporates textual input as supplementary information for segmentation. Figure 1(b) illustrates medical image segmentation with textual prompts, wherein diagnostic texts provided by physicians serve as language prompting. The task involves inputting a medical image along with its corresponding diagnostic text and outputting segmentation results for all lesions present [20]. However, in clinical practice, physicians often need to segment specific lesions to aid in diagnosis and treatment, thus rendering conventional medical image segmentation methods inadequate for practical

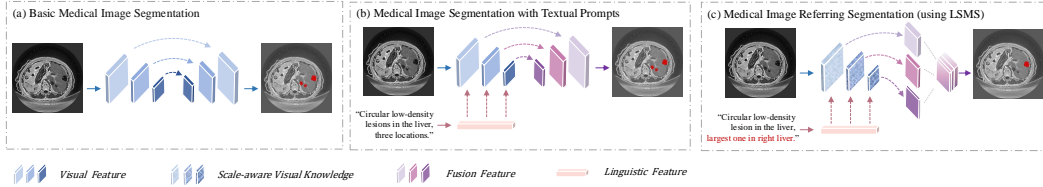


Figure 1: Comparison between Medical Image Referring Segmentation and conventional medical image segmentation tasks, illustrating the distinction in feature handling process between the proposed LSMS and existing medical segmentation methods. In the images displaying segmentation results, the regions highlighted in red represent the Ground Truth. For intuitive correspondence with the left-right references in the text, all CT images in this paper have been mirrored horizontally.

applications. Language, as a convenient medium for expressing physicians’ needs, can be used to indicate target segmentation objects. Therefore, we introduce the task of Medical Image Referring Segmentation (MIRS), where medical images are accompanied by language expressions that indicate specific lesions within the images. Figure 1(c) represents the introduced task, MIRS, which aims to specifically output segmentation results for the lesion referenced in the language expressions. In the example depicted in the figure, segmentation of the largest lesion in the right liver is required.

Deep learning methods have demonstrated outstanding performance in image segmentation tasks. As illustrated in Figure 1(a), classical medical image segmentation often relies on architectures such as U-Net [29] or Transformer [32]. These approaches involve down-sampling feature maps to acquire high-level contextual information, followed by up-sampling to reconstruct spatial dimensions [3, 2]. To further enhance segmentation performance, approaches incorporating language prompting have emerged [20], as depicted in Figure 1(b). These methods fuse visual and linguistic features during the encoding stage of the model, aiding in the acquisition of additional contextual information. The latest referring segmentation methods in natural images also utilize the similar architecture [39]. However, due to the varying size and shape inherent in medical images, the fusion of single-scale representations at each stage with linguistic features alone is insufficient for precise object localization. Moreover, the sequential structure adopted in the decoding stage lacks a comprehensive understanding of features at various scales, thereby constraining segmentation performance.

Upon analyzing the requirements of the MIRS task and previous efforts in medical image segmentation, we identify two primary challenges in MIRS: (i) Robust vision-language modeling. The considerable differences in size and shape among objects in the medical visual environment present a challenge for effectively integrating visual and linguistic features. Fusion between linguistic features and single-scale visual features may overlook the rich local visual information correlated with linguistic guidance, thereby impacting the model’s object localization performance. (ii) Comprehensive multi-scale interaction. Globally modeling the complex differences across scales enables the extraction of valuable global visual-linguistic features. Given the complexity of the visual environment in medical images, a lack of complementary information between scales may result in insufficient capability to identify lesion boundaries during segmentation.

To address these challenges, we propose a novel MIRS architecture (feature handling process shown in Figure 1(c)), namely **Language-guided Scale-aware MedSegmentor (LSMS)**. Within LSMS, we introduce a **Scale-aware Vision-Language Attention (SVLA)** module embedded in the encoder block. SVLA enhances the acquisition of scale-aware visual knowledge by employing convolutional kernels of various sizes, facilitating close interaction with linguistic features and thereby improving visual-linguistic consistency. As shown in Figure 2, LSMS (w/o FSD) equipped with SVLA exhibits a significant enhancement in lesion localization capability compared to the results of existing vision-language model LViT [20] and LAVT [39]. Additionally, we devise a **Full-Scale Decoder (FSD)** that globally models multi-modal information by aligning and integrating multi-modal feature maps from various scales, thereby enhancing the comprehension of details within complex medical visual environment.

In Figure 2, LSMS, when contrasted with LSMS (w/o FSD), exhibits a more precise prediction of lesion boundaries during segmentation.

The proposed MIRS task lacks an available dataset, necessitating a corresponding language expression for the localization of each lesion in medical images. Therefore, we developed the Reference Hepatic

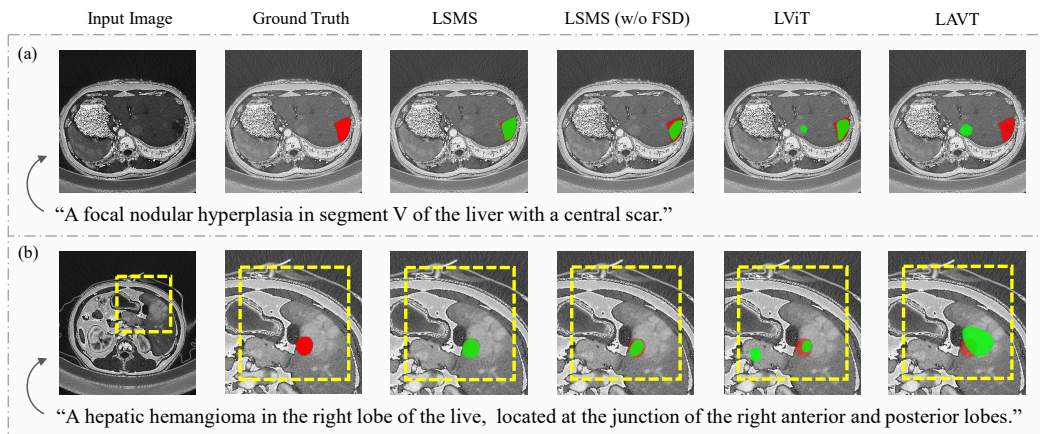


Figure 2: Qualitative results of different approaches. The red regions denote the Ground Truth, while the green regions represent the segmentation results of our LSMS, LSMS (w/o FSD), LViT [20] and LAVT [39]. In sample (b), for ease of observation, the key region within the image have been enlarged, with a yellow rectangular box serving as a reference for location.

Lesion Segmentation (RefHL-Seg) dataset, comprising 2,283 abdominal CT slices from 231 cases. With the assistance of radiologists, we annotated abdominal CT images containing liver lesions, providing language expressions for each lesion regarding its morphology, location, type, and other relevant information. Additionally, corresponding segmentation masks were delineated to facilitate training and validation for the MIRS task.

In summary, our contributions encompass four aspects:

1. We introduce the novel task of MIRS, which entails locating and segmenting target objects in medical images based on reference expressions. The application of MIRS in clinical practice can enhance diagnostic efficiency for physicians.
2. We propose a model named LSMS for the MIRS task, comprising a SVLA module to improve object localization capability and a full-scale decoder to enhance the accuracy of lesion boundary prediction during segmentation.
3. We develop the Reference Hepatic Lesion Segmentation (RefHL-Seg) dataset for training and validating the MIRS task. RefHL-Seg consists of 2,283 abdominal CT slices from 231 cases.
4. We conduct comprehensive experiments on the RefHL-Seg dataset for MIRS, as well as on datasets for conventional medical image segmentation tasks. Experimental results demonstrate the superiority of LSMS over current state-of-the-art methods with lower computational costs.

2 Related Works

2.1 Medical Image Segmentation

For medical image segmentation tasks, early methods [22, 4, 38] extended from image classification networks to achieve semantic segmentation, among which the Fully Convolutional Network (FCN) [22] is an end-to-end semantic segmentation network [18]. Multi-scale architectures have been proven to enhance segmentation performance based on CNN methods. U-Net [29] is considered a pioneer in medical image segmentation. U-Net++ [43] further improved U-Net by enhancing skip connections to bridge the semantic gap between shallow encoder layers and deep decoder layers. MS-DualGuided [30] focused on both spatial and channel dimensions of feature maps at different scales. CA-Net [34] proposed a multi-scale context-aware network for multi-modal medical image segmentation. Subsequently, the introduction of Transformer [32] was found to enhance medical image segmentation performance. TransUNet [3] integrated the power of Transformers with the U-Net architecture for improved instance segmentation. Swin-UNet [2] specifically designed to leverage the hierarchical features and shifted window mechanisms of Swin Transformer [21], thereby

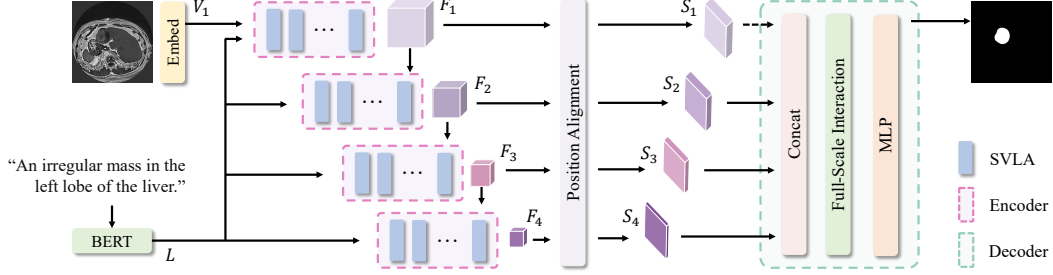


Figure 3: An illustration of LSMS. Initially, the input image and the reference expression are embedded separately through the visual embedding block and the BERT [6] language encoder, yielding visual feature V_1 and linguistic feature L , which are then fed into the language-guided vision encoder. The encoder incorporates the Scale-aware Vision-Language Attention (SVLA) module to interact between visual knowledge from different receptive fields and linguistic features. The encoders at each stage learn rich multi-modal features $F_i, i \in \{1, 2, 3, 4\}$. Through the Position Alignment module, $F_i, i \in \{1, 2, 3, 4\}$ uniformly resize the feature maps of various scales while preserving channel disparities, resulting in $S_i, i \in \{1, 2, 3, 4\}$. Features $S_i, i \in \{2, 3, 4\}$ are then globally modeled across scales by the full-scale decoder for final segmentation.

enhancing the model’s capability to capture both local and global context. Furthermore, LViT [20] proposed a medical image segmentation model with language prompting. These methods acquire feature maps through progressively down-sampling, yielding low-resolution representations. And they utilize a sequential up-sampling structure in the decoding stage, lacking a global understanding of multi-scale knowledge.

2.2 Vision-Language Segmentation Models

The capability of vision-language models to encode rich multi-modal representations has played a crucial role in the field of computer vision [35, 42]. ViLT [17], by simplifying the processing of visual inputs in CLIP [28], proposed a more parameter-efficient architecture. This architecture enables interaction layers to handle visual features effectively without relying on separate deep visual embeddings. Subsequently, there have been significant research efforts in image segmentation [19], where text information is utilized to enhance model segmentation capabilities. VLT [7] and EFN [9] utilize a Transformer-based encoder-decoder framework, employing attention mechanisms in decoding stages to augment contextual information for natural image referring segmentation. LAVT [39] adopted an early fusion approach, modeling multi-modal context within the Vision Transformer (ViT) [8] encoder. Some methods [1, 24] have started using text information to assist in medical image analysis. [27] leveraged the knowledge transfer ability of pretrained vision-language models [18] to the medical domain by employing well-designed medical prompts. LViT [20] introduced textual prompts as auxiliary information during the encoding stage for segmentation. Due to the complexity of medical visual environment, existing methods struggle to achieve explicit alignment between text and images. To address this, we propose a design involving close interaction between scale-aware visual knowledge and linguistic features to facilitate modeling of visual-linguistic relationships.

3 Language-Guided Scale-Aware Medical Segmentor

3.1 Overview

In the proposed Language-guided Scale-aware MedSegmentor (LSMS), we learn visual knowledge from diverse receptive fields and tightly engage with linguistic features. Subsequently, leveraging a full-scale decoder, we globally model multi-modal information across all scales, thereby facilitating MIRS task. The overall architecture of LSMS is presented in Figure 3.

Given an image and a language expression, our model predicts the segmentation mask corresponding to the language reference. Our LSMS follows a workflow composed of *[language-guided vision encoder]* - *[position alignment]* - *[full-scale decoder]*. LSMS comprises four stages, each with varying numbers of encoder blocks and different feature map resolutions. The encoder (Section

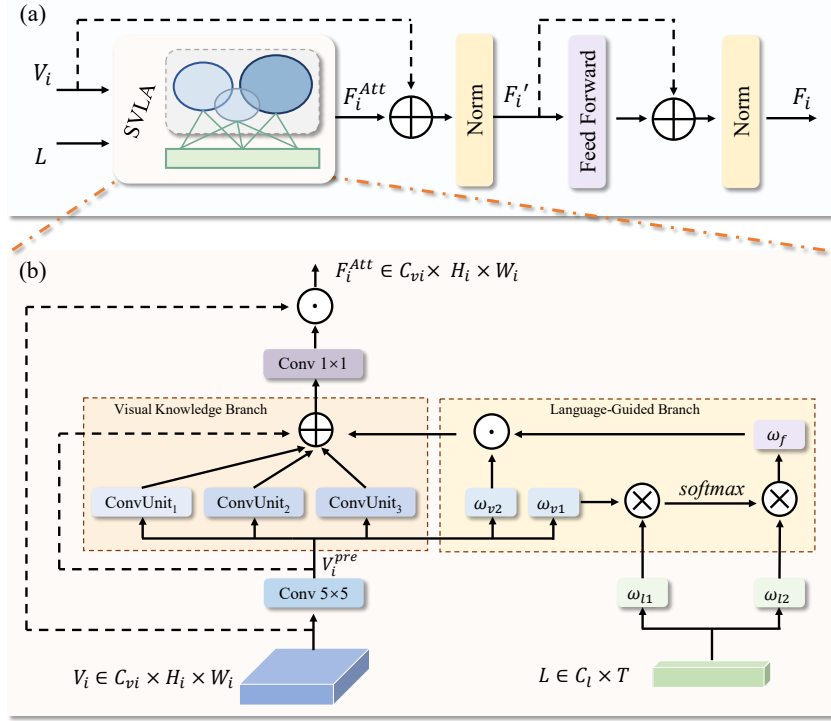


Figure 4: (a) An illustration of the encoder block in the Language-Guided Vision Encoder. (b) An illustration of the Scale-aware Vision-Language Attention.

3.2) incorporates a novel scale-aware vision-language attention module (Section 3.3), which learns rich visual knowledge through convolutions of different sizes and closely interacts with linguistic features. Additionally, we propose a full-scale decoder (Section 3.4) to globally model multi-modal information across multiple scales, enhancing the understanding of context details. In the following subsections, we elaborate on each component of LSMS.

3.2 Language-Guided Vision Encoder

To facilitate deep interaction between linguistic features and the complex visual environment of medical images, our encoder leverages a novel attention module (Section 3.3) to perceive visual details in the image under linguistic guidance, thus obtaining valuable multi-modal representations.

As illustrated in Figure 3, our encoding phase comprises four stages with decreasing feature map resolutions. The i -th stage consists of N_i encoder blocks. For the sake of clarity, we assume that $N_i = 1, i \in \{1, 2, 3, 4\}$ in this section. LSMS receives an input image alongside a reference expression. We extract the linguistic feature $L \in \mathbb{R}^{C_l \times T}$ using the language encoder BERT [6], where T denotes the number of words, and C_l represents the channel number of the linguistic feature. Similarly, the input image undergoes an embedding block to yield the initial visual input $V_1 \in \mathbb{R}^{C_{v1} \times H_1 \times W_1}$ for the encoder, where H_1 and W_1 represent the height and width of the visual feature, and C_{v1} represents the channel number. Each stage comprises a down-sampling block and a stack of encoder blocks. For each stage, the aggregation of the multi-modal feature maps $F_i \in \mathbb{R}^{C_{vi} \times H_i \times W_i}$ can be expressed as:

$$F_i = \begin{cases} LGVE(V_1, L), & i = 1 \\ LGVE(Down(F_{i-1}), L), & i = 2, 3, 4 \end{cases} \quad (1)$$

where i denotes the index of the stage, the function $Down(\cdot)$ represents the down-sampling block, and $LGVE(\cdot)$ denotes the encoder block. The visual input provided to the encoder block is obtained by $V_i = Down(F_{i-1})$. The down-sampling block consists of a convolutional layer with a stride of 2 and a kernel size of 3×3 , followed by batch normalization.

As depicted in Figure 4(a), the architecture of encoder blocks follows the design of ViT [8], but we introduce a SVLA module (Section 3.3) to replace the conventional self-attention mechanism. The workflow of the encoder block is illustrated by the following:

$$F'_i = \text{Norm}(\text{SVLA}(V_i, L) + V_i), \quad (2)$$

$$F_i = \text{Norm}(\text{FeedForward}(F'_i) + F'_i), \quad (3)$$

where $\text{Norm}(\cdot)$ and $\text{FeedForward}(\cdot)$ represent normalization and feed forward layers, $\text{SVLA}(\cdot)$ denotes SVLA module, and the output of $\text{SVLA}(V_i, L)$ is labeled as F_i^{Att} .

3.3 Scale-aware Vision-Language Attention

In medical images, instances vary greatly in size and shape, posing a challenge in pinpointing lesions referred to linguistic cues within intricate visual contexts. Addressing this, we learn scale-aware visual knowledge from diverse receptive fields by employing convolutional kernels of varying sizes, integrating linguistic features with visual knowledge across multiple scales.

As depicted in Figure 4(b), our proposed attention mechanism, termed Scale-aware Vision-Language Attention (SVLA), initially captures preliminary visual features through a convolution operation, and then employs Visual Knowledge Branch and the Language-Guided Branch to model rich visual knowledge and visual-linguistic relationships, followed by a 1×1 convolution operation to learn the interplay between the branches. In i -th stage, with visual input $V_i \in \mathbb{R}^{C_{vi} \times H_i \times W_i}$ and language input $L \in \mathbb{R}^{C_l \times T}$, we obtain the preliminary visual feature map $V_i^{\text{pre}} \in \mathbb{R}^{C_{vi} \times H_i \times W_i}$ by the formula $V_i^{\text{pre}} = \text{Conv}_{5 \times 5}(V_i)$.

Visual Knowledge Branch To accommodate the characteristics of medical image visual environment, we devised ConvUnits to capture scale-aware visual knowledge. ConvUnits comprises diverse convolution kernels, with each unit consisting of a $1 \times d_j$ and a $d_j \times 1$ convolution operations, where $j \in \{1, 2, 3\}$. Each SVLA module comprises three ConvUnits, aimed at capturing scale-aware visual knowledge from various receptive fields. Visual knowledge $\text{Att}_i^V \in \mathbb{R}^{C_{vi} \times H_i \times W_i}$ can be derived using the following formula:

$$\text{Att}_i^V = \sum_{j=1}^3 \text{ConvUnit}_j(V_i^{\text{pre}}), \quad (4)$$

where $\text{ConvUnit}_j(\cdot)$ indicates j -th ConvUnit. The rectangular convolution kernels in ConvUnits enable the acquisition of detailed visual information with low computational costs.

Language-Guided Branch We employ the Language-Guided Branch to model relationships between linguistic information and various visual coordinates, facilitating the guidance of lesion localization in complex visual environment. The steps to obtain language-guided knowledge $\text{Att}_i^L \in \mathbb{R}^{C_{vi} \times H_i \times W_i}$ are as follows:

$$V_{i1}, V_{i2} = \text{flatten}(\omega_{v1}(V_i^{\text{pre}}), \omega_{v2}(V_i^{\text{pre}})), \quad (5)$$

$$L_{i1}, L_{i2} = \omega_{l1}(L), \omega_{l2}(L), \quad (6)$$

$$\alpha_i = V_{i1}^\top L_{i1}, \quad (7)$$

$$\text{Att}_i^{L'} = \text{unflatten}((\text{softmax}(\frac{\alpha_i}{\sqrt{C_l}})L_{i2}^\top)^\top), \quad (8)$$

$$\text{Att}_i^L = \omega_f(\text{Att}_i^{L'}) \odot V_{i2}, \quad (9)$$

where ω_{v1} , ω_{v2} , ω_{l1} , ω_{l2} , ω_f are projection functions, $\text{flatten}(\cdot)$ denotes the operation of flattening the two spatial dimensions into a single dimension along the rows, $\text{unflatten}(\cdot)$ indicates the opposite operation of $\text{flatten}(\cdot)$, and \odot is element-wise matrix multiplication operation. ω_{l1} and ω_{l2} each is implemented as a 1×1 convolution, yielding channels of size C_{vi} . ω_{v1} , ω_{v2} and ω_f each is defined as a 1×1 convolution and an instance normalization.

Table 1: Detailed settings of different stages in our LSMS.

	Stage 1	Stage 2	Stage 3	Stage 4
number of blocks (N_i)	3	3	5	2
visual output size	$\frac{H}{4} \times \frac{W}{4}$	$\frac{H}{8} \times \frac{W}{8}$	$\frac{H}{16} \times \frac{W}{16}$	$\frac{H}{32} \times \frac{W}{32}$
channel	64	128	320	512

Comprehensive Attention We integrate information from the Visual Knowledge Branch and the Language-Guided Branch to compute comprehensive attention weights through convolution, thereby reweighting the input V_i to the SVLA module. The feature $F_i^{Att} \in \mathbb{R}^{C_{vi} \times H_i \times W_i}$ is obtained using the following:

$$F_i^{Att} = Conv_{1 \times 1}(V_i^{pre} + Att_i^V + Att_i^L) \odot V_i, \quad (10)$$

where $Conv_{1 \times 1}$ represents the 1×1 convolution operation, and \odot is element-wise matrix multiplication operation.

3.4 Full-Scale Decoder

In order to integrate linguistic cues for comprehending complex medical visual environment, a comprehensive cross-scale understanding of visual-linguistic contexts is necessary. Therefore, we devised a Full-Scale Decoder (FSD) to capture high-level semantics following the encoder. Unlike previous methods [41, 37, 10] with sequential structures, we globally process multi-modal features of various scales after aligning their positions. We employ Position Alignment to map them to the same feature map size of F_1 while retaining their original channel numbers. Subsequently, we concatenate features from different scales, pass them through a lightweight InterScale block for globally modeling multi-scale contexts, and finally generate segmentation predictions. The process is as follows:

$$S_1, S_2, S_3, S_4 = PositionAlign(F_1, F_2, F_3, F_4), \quad (11)$$

$$Out = Seg(InterScale(Concat[S_2, S_3, S_4])), \quad (12)$$

where $PositionAlign(\cdot)$ represents the Position Alignment operation, $InterScale(\cdot)$ is implemented as a lightweight Hamburger [11] function, and $Seg(\cdot)$ indicates a 1×1 convolution and an up-sampling function for final prediction. $PositionAlign(\cdot)$ is realized through bilinear interpolation operations.

It is noteworthy that we exclusively utilize features generated from 2, 3, 4-th stages for global decoding. This choice is informed by the observation that the shallow features from the first stage exhibit a lower degree of visual-linguistic consistency, encompassing redundant information from irrelevant regions in the images. This redundancy hampers lesion localization and hinders segmentation. The efficacy of this design will be validated in the Ablation Study (Section 4.5) and further elucidated through visualization analysis (Section 4.6) to comprehend the disparities and characteristics of features from different stages.

4 Experiments

4.1 Datasets

We conducted experiments on three datasets to assess the performance of LSMS: our self-established dataset, **Reference Hepatic Lesion Segmentation (RefHL-Seg)**, as well as MosMedData+ [23, 14] and QaTa-COV19 [5] datasets.

RefHL-Seg represents the first dataset tailored specifically for the MIRS task. RefHL-Seg comprises 2,283 abdominal CT slices from 231 cases, predominantly featuring lesions such as Hemangiomas, Liver Cysts, Hepatocellular Carcinomas (HCC), Focal Nodular Hyperplasia, and Metastasis. With collaboration from radiology experts, we meticulously annotated all liver lesions for the first time, providing detailed descriptions of their locations and morphologies. Each lesion’s textual annotation includes information such as liver segment (location), diameter, shape, boundary, enhancement pattern, lesion type, and more. An exemplary textual annotation containing all relevant information

Table 2: Experimental results on the RefHL-Seg, QaTa-COV19 and MosMedData+ datasets in terms of Dice and mIoU. The best scores are in red, and the secondbest scores are in blue.

Method	Backbone	Text	Param (M)	Flops (G)	RefHL-Seg		QaTa-COV19		MosMedData+	
					Dice (%)	mIoU (%)	Dice (%)	mIoU (%)	Dice (%)	mIoU (%)
U-Net [29]	CNN	×	14.8	50.3	48.67	37.89	79.02	69.46	64.60	50.73
UNet++ [43]	CNN	×	74.5	94.6	51.84	40.27	79.62	70.25	71.75	58.39
AttUNet [25]	CNN	×	34.9	101.9	50.67	40.11	79.31	70.04	66.34	52.82
nnUNet [16]	CNN	×	19.1	412.7	51.63	41.89	80.42	70.81	72.59	60.36
TransUNet [3]	Hybrid	×	105	56.7	52.33	44.76	78.63	69.13	71.24	58.44
Swin-Unet [2]	Hybrid	×	82.3	67.3	51.34	44.26	78.07	68.34	63.29	50.19
UCTransNet [33]	Hybrid	×	65.6	63.2	54.87	44.38	79.15	69.60	65.90	52.69
LViT [20]	Hybrid	×	28.0	54.0	54.84	44.65	81.12	71.37	72.58	60.40
LSMS	Hybrid	×	8.78	8.91	58.75	49.39	82.14	72.07	73.14	61.76
ConVIRT [40]	CNN	✓	35.2	44.6	61.37	53.56	79.72	70.58	72.06	59.73
TGANet [31]	CNN	✓	19.8	41.9	63.28	55.49	79.87	70.75	71.81	59.28
GLoRIA [15]	Hybrid	✓	45.6	60.8	63.69	55.82	79.94	70.68	72.42	60.18
VILT [17]	Hybrid	✓	87.4	55.9	64.58	56.65	79.63	70.12	72.36	60.15
CLIP [28]	Hybrid	✓	87.0	105.3	68.76	60.33	79.81	70.66	71.97	59.64
LAVT [39]	Hybrid	✓	118.6	83.8	69.03	60.98	79.28	69.89	73.29	60.41
SLViT [26]	Hybrid	✓	133.6	52.2	71.94	62.83	80.68	71.57	73.08	60.11
LViT [20]	Hybrid	✓	29.7	54.1	71.48	62.02	83.66	75.11	74.57	61.33
LSMS (1/4)	Hybrid	25%	8.78	8.91	77.57	68.95	83.39	75.09	76.47	65.05
LSMS (1/2)	Hybrid	50%	8.78	8.91	77.63	69.14	83.44	75.13	76.98	65.71
LSMS	Hybrid	100%	8.78	8.91	78.14	70.22	84.05	75.70	77.88	66.83

is provided as follows: "A vascular tumor in the VI segment of the liver, with a diameter of 7.5mm, irregular shape, clear boundary, and no ring enhancement." Additionally, experiments will involve testing language expressions that contain only partial information sufficient for lesion localization, such as "A vascular tumor in the VI segment of the liver, with an irregular shape."

The MosMedData+ [23, 14] and QaTa-COV19 [5] datasets are established datasets for conventional medical image segmentation tasks. [20] extended the textual annotations of these datasets, serving for the evaluation of Medical Image Segmentation with Textual Prompts. The MosMedData+ dataset comprises 2,729 CT scan slices of lung infections, primarily containing information about the location of lung infections and the number of infected regions. The QaTa-COV19 dataset consists of 9,258 chest X-ray images manually annotated with COVID-19 lesions, focusing on whether both lungs are infected, the quantity of lesions, and the approximate location of the infected regions.

4.2 Evaluation Metric

In line with prior research [20], we utilize the Dice score and mean Intersection-over-Union (mIoU) to assess the effectiveness of our proposed method. The Dice score quantifies performance by calculating the intersection of the predicted results and the ground truth, divided by twice the sum of the sizes of the two sets. The mIoU computes the average Intersection over Union for multiple segmentation instances, providing an overall measure of segmentation accuracy across all instances.

4.3 Implementation Details

The proposed LSMS is implemented using PyTorch, leveraging the BERT implementation from the HuggingFace Transformer library [36]. Regarding dataset partitioning, we separated the original training set into training and validation sets. For the convolutional layers in the Visual Knowledge Branch of SVLA, we initialized the weights using SegNeXt [12] pre-trained on ImageNet-22K [13]. The language encoder of our model was initialized with the official pre-trained BERT weights, consisting of 12 layers with a hidden size of 768. The number of encoder blocks and feature dimensions for each stage are presented in Table 1. For the convolutional branch of SVLA, we used kernel sizes of $d_1 = 7$, $d_2 = 11$, and $d_3 = 21$. The remaining weights in our model were randomly initialized.

Subsequently, we employed the AdamW optimizer with a weight decay of 0.01. The learning rate was initialized to $3e-5$ and scheduled using polynomial decay with a power of 0.9. All models were

Table 3: Ablation studies on the RefHL-Seg val set. The optimal scores are highlighted in red.

				Dice	mIoU					Dice	mIoU
(a) Kernel size of a single ConvUnit in SVLA						(c) Ablation on FSD					
$d_1 = 5$				72.95	64.14	LSMS (w/o FSD)				74.86	65.64
$d_1 = 7$				73.28	64.81	LSMS (w/ FSD)				78.14	70.22
$d_2 = 11$				74.03	65.27	(d) Ablation on design choices of FSD					
$d_2 = 15$				73.97	65.31	S_4 -Head-MLP				75.82	67.39
$d_3 = 19$				72.33	63.97	S_1, S_2, S_3, S_4 -MLP-Concat-MLP				77.07	68.48
$d_3 = 21$				73.36	65.22	S_1, S_2, S_3, S_4 -Concat-Head-MLP				77.95	69.33
						S_1, S_2, S_3, S_4 -MLP-Concat-Head-MLP				76.35	68.21
(b) Ablation on design choices of SVLA						(e) FSD on various stages					
ConvU1	ConvU2	ConvU3	PM			S_1	S_2	S_3	S_4		
✓	✓			76.34	66.96				✓	77.82	66.39
✓		✓		76.52	67.03			✓	✓	78.71	67.26
	✓	✓		76.44	67.17	✓	✓	✓		77.83	66.92
✓	✓	✓		77.10	68.88		✓	✓	✓	78.14	70.22
✓	✓	✓	✓	78.14	70.22	✓	✓	✓	✓	77.95	69.33

trained for 100 epochs with a batch size of 16. Images were uniformly resized to 480×480 before inputting into the model, with no additional data augmentation applied.

4.4 Comparison with the State-of-the-Arts

Classical Medical Image Segmentation We compared the performance of LSMS with existing segmentation models on the RefHL-Seg, QaTa-COV19, and MosMedData+ datasets, as shown in Table 2. In scenarios where language input is not utilized, we observed that LSMS outperformed all existing methods in classical medical image segmentation task while minimizing computational costs. This underscores the efficiency and superiority of LSMS in understanding medical visual environment.

Medical Image Segmentation with Textual Prompts The QaTa-COV19 and MosMedData+ datasets are primarily utilized for training and validating Medical Image Segmentation with Textual Prompts. In Table 2, our LSMS achieves state-of-the-art (SOTA) performance for this task, particularly improving Dice by 3.21% and mIoU by 5.50% on the MosMedData+ dataset. This indicates that LSMS, with the assistance of textual descriptions, can complement visual information with linguistic cues, leading to more accurate segmentation of all lesions in the images and thereby achieving superior outcomes.

Medical Image Referring Segmentation The RefHL-Seg dataset we constructed serves the specific purpose of training and validating the MIRS task. Each sample in the dataset necessitates the model to segment the particular lesion indicated by the reference expression, thus rendering the performance of all methods suboptimal when text input is absent. When provided with complete inputs containing both text and images, our LSMS significantly improves accuracy compared to all existing models. Specifically, compared to the previous SOTA method LViT [20], LSMS achieves an increase of 6.66% in Dice and 7.80% in mIoU. This improvement stems from LSMS’s enhanced understanding of the complex medical visual environment and its precise localization capability based on linguistic cues. In Table 2, LSMS (1/4) and LSMS (1/2) denote the models tested with only 25% and 50% of the textual input, respectively, by omitting portions such as size or shape descriptions. The results indicate that LSMS still outperforms existing methods significantly. This underscores that our LSMS, trained to precisely locate specified lesions in images with minimal textual assistance, exhibits outstanding language-guided lesion localization capability.

4.5 Ablation Study

Kernel size of a single ConvUnit in SVLA We have meticulously evaluated the performance of using different convolutional kernels in SVLA on the validation set of RefHL-Seg, as illustrated in

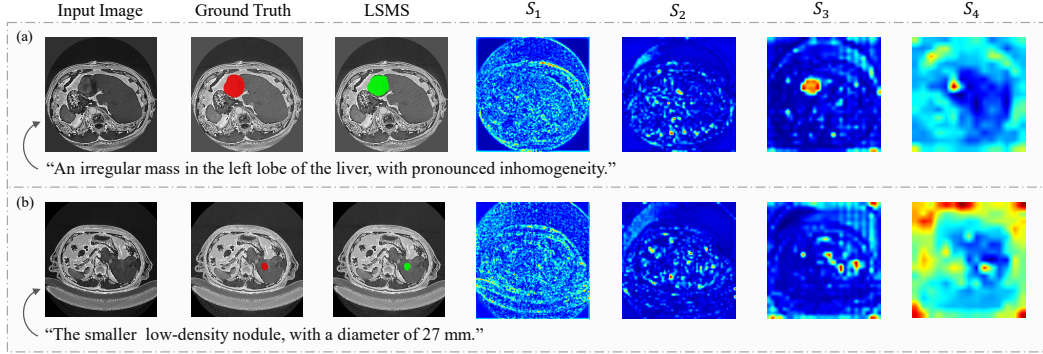


Figure 5: Visualization of the feature maps from different stages in LSMS. The red regions denote the Ground Truth, while the green regions represent the segmentation results of our LSMS.

Table 3(a). $d_j = N$ indicates the ConvUnit containing a $1 \times N$ convolution and a $N \times 1$ convolution. The strip-like convolution kernels aim to obtain detailed local visual information with low costs. We employed a single ConvUnit in SVLA to evaluate the impact of various convolution kernel sizes d_j . In Table 3(a), sizes 7 and 21 show superior performance among those with comparable computational costs. The performance of medium-size convolution kernels is similar, so we choose size 11 due to its lower computational cost. The utilization of diverse convolution kernels can aid in capturing features from varying receptive fields, which helps in extracting rich local visual features. We opted for kernel sizes of $d_1 = 7$, $d_2 = 11$, and $d_3 = 21$ as alternatives.

Ablation on SVLA design In Table 3(b), ConvUnit $_j$ comprises a $1 \times d_j$ convolution and a $d_j \times 1$ convolution, *PixelMap* represents a element-wise matrix multiplication operation in the Language-Guided Branch. Table 3(b) shows that the deployment of three ConvUnits produces the most favorable outcomes, and the incorporation of the *PixelMap* enhances language-guided visual knowledge, significantly boosting segmentation accuracy.

Effectiveness of FSD To assess the effectiveness of the FSD, we compared the performance of the complete LSMS with LSMS (w/o FSD), and the results are reported in Table 3(c). Experimental findings indicate that removing the FSD module leads to performance degradation, with Dice decrease of 3.28% and mIoU decrease of 4.58%, respectively. Furthermore, FSD incurs only a modest increase of 2.1M parameters and 1.7G Flops, yet significantly enhances performance. This underscores its efficiency in boosting performance by globally modeling multi-modal information.

Ablation on FSD design To validate the effectiveness of the individual components in the design of FSD, we conducted ablation experiments on its constituents, as presented in Table 3(d). It is evident that relying solely on features from the final stage is insufficient, and while adding MLP layers before concatenation increases complexity, it results in the loss of valuable information from each stage. The incorporation of the Hamburger Head design enhances the ability to globally model multi-scale information, consequently improving segmentation performance. The S_1, S_2, S_3, S_4 -Concat-Head-MLP design demonstrates the best performance.

FSD on various stages Given the multi-modal features from different stages after Position Alignment, FSD concatenates them and performs joint refinement in a single forward pass. Here, S_i , $i \in \{1, 2, 3, 4\}$, denotes the multi-modal features input to FSD from the i -th stage. Table 3(e) compares multiple input sequences, confirming the value of multi-scale interaction for global reasoning. As shown, S_2, S_3, S_4 exhibit optimal performance for FSD. This superiority is attributed to the insufficient depth of interaction between visual information and linguistic cues in the shallow feature S_1 , which include irrelevant information and hindering the localization and segmentation of specified lesions. Conversely, the latter three layers demonstrate strong visual-linguistic consistency, facilitating favorable predictions. Visualization analysis of each feature map is detailed in Section 4.6.

4.6 Visualization Analysis

In Figure 5, we illustrate segmentation results and feature maps obtained from two sets of inputs, denoted as (a) and (b). In Figure 5(a), the language expression is “An irregular mass in the left lobe of the liver, with pronounced inhomogeneity.” The language expression for Figure 5(b) is “The smaller low-density nodule, 27 mm in diameter.” The labels $S_i, i \in \{1, 2, 3, 4\}$ represent encoded multi-modal features from different stages. The segmentation results demonstrate LSMS’s ability to accurately locate and segment the specified lesions based on the language expressions. Analyzing $S_i, i \in \{1, 2, 3, 4\}$ reveals LSMS’s progressive focus from shallow to deep layers onto the corresponding lesions: S_1 comprehends the overall visual context, S_2 extensively attends to various objects within the image, S_3 narrows down to candidate lesions, and S_4 precisely focuses on the lesion specified by the language input. In sample (a), where only one large lesion is present, S_3 rapidly focuses on the target area. As modeling deepens, S_4 demonstrates profound visual-linguistic cues. In sample (b), where multiple lesions coexist in the image, S_3 exhibits multiple attention points. Through further vision-language interaction, S_4 can focus on the lesions specified by the expression, aiding the model in making correct predictions.

5 Conclusion

In this paper, we introduce a novel task, Medical Image Referring Segmentation, driven by clinical demands. And we propose the LSMS model with two appealing designs. LSMS integrates a novel attention mechanism to enhance object localization by tightly interacting scale-aware visual knowledge and linguistic cues. We introduce a full-scale decoder for global modeling of multi-modal features, improving boundary prediction in segmentation. Additionally, we develop the RefHL-Seg dataset for training and validating the MIRS task. Our experimental results show LSMS outperforms current methods in both MIRS and conventional medical image segmentation tasks with lower computational costs.

References

- [1] Riddhish Bhalodia, Ali Hatamizadeh, Leo Tam, Ziyue Xu, Xiaosong Wang, Evrim Turkbey, and Daguang Xu. Improving pneumonia localization via cross-attention on medical images and reports. In *Medical Image Computing and Computer Assisted Intervention–MICCAI 2021: 24th International Conference, Strasbourg, France, September 27–October 1, 2021, Proceedings, Part II 24*, pages 571–581. Springer, 2021.
- [2] Hu Cao, Yueyue Wang, Joy Chen, Dongsheng Jiang, Xiaopeng Zhang, Qi Tian, and Manning Wang. Swin-UNET: UNet-like pure transformer for medical image segmentation. In *European conference on computer vision*, pages 205–218. Springer, 2022.
- [3] Jieneng Chen, Yongyi Lu, Qihang Yu, Xiangde Luo, Ehsan Adeli, Yan Wang, Le Lu, Alan L Yuille, and Yuyin Zhou. TransUNet: Transformers make strong encoders for medical image segmentation. *arXiv preprint arXiv:2102.04306*, 2021.
- [4] Liang-Chieh Chen, George Papandreou, Iasonas Kokkinos, Kevin Murphy, and Alan L Yuille. Deeplab: Semantic image segmentation with deep convolutional nets, atrous convolution, and fully connected crfs. *IEEE transactions on pattern analysis and machine intelligence*, 40(4):834–848, 2017.
- [5] Aysen Degerli, Serkan Kiranyaz, Muhammad EH Chowdhury, and Moncef Gabbouj. Osegnet: Operational segmentation network for covid-19 detection using chest x-ray images. In *2022 IEEE International Conference on Image Processing (ICIP)*, pages 2306–2310. IEEE, 2022.
- [6] Jacob Devlin, Ming-Wei Chang, Kenton Lee, and Kristina Toutanova. Bert: Pre-training of deep bidirectional transformers for language understanding. *arXiv preprint arXiv:1810.04805*, 2018.
- [7] Henghui Ding, Chang Liu, Suchen Wang, and Xudong Jiang. Vision-language transformer and query generation for referring segmentation. In *Proceedings of the IEEE/CVF International Conference on Computer Vision*, pages 16321–16330, 2021.

- [8] Alexey Dosovitskiy, Lucas Beyer, Alexander Kolesnikov, Dirk Weissenborn, Xiaohua Zhai, Thomas Unterthiner, Mostafa Dehghani, Matthias Minderer, Georg Heigold, Sylvain Gelly, et al. An image is worth 16x16 words: Transformers for image recognition at scale. *arXiv preprint arXiv:2010.11929*, 2020.
- [9] Guang Feng, Zhiwei Hu, Lihe Zhang, and Huchuan Lu. Encoder fusion network with co-attention embedding for referring image segmentation. In *Proceedings of the IEEE/CVF Conference on Computer Vision and Pattern Recognition*, pages 15506–15515, 2021.
- [10] Jun Fu, Jing Liu, Haijie Tian, Yong Li, Yongjun Bao, Zhiwei Fang, and Hanqing Lu. Dual attention network for scene segmentation. In *Proceedings of the IEEE/CVF conference on computer vision and pattern recognition*, pages 3146–3154, 2019.
- [11] Zhengyang Geng, Meng-Hao Guo, Hongxu Chen, Xia Li, Ke Wei, and Zhouchen Lin. Is attention better than matrix decomposition? *arXiv preprint arXiv:2109.04553*, 2021.
- [12] Meng-Hao Guo, Cheng-Ze Lu, Qibin Hou, Zhengning Liu, Ming-Ming Cheng, and Shi-min Hu. Segnext: Rethinking convolutional attention design for semantic segmentation. In S. Koyejo, S. Mohamed, A. Agarwal, D. Belgrave, K. Cho, and A. Oh, editors, *Advances in Neural Information Processing Systems*, volume 35, pages 1140–1156. Curran Associates, Inc., 2022.
- [13] Meng-Hao Guo, Cheng-Ze Lu, Qibin Hou, Zhengning Liu, Ming-Ming Cheng, and Shi-Min Hu. Segnext: Rethinking convolutional attention design for semantic segmentation. *arXiv preprint arXiv:2209.08575*, 2022.
- [14] Johannes Hofmanninger, Florian Prayer, Jeanny Pan, Sebastian Röhrich, Helmut Prosch, and Georg Langs. Automatic lung segmentation in routine imaging is primarily a data diversity problem, not a methodology problem. *European Radiology Experimental*, 4:1–13, 2020.
- [15] Shih-Cheng Huang, Liyue Shen, Matthew P Lungren, and Serena Yeung. Gloria: A multimodal global-local representation learning framework for label-efficient medical image recognition. In *Proceedings of the IEEE/CVF International Conference on Computer Vision*, pages 3942–3951, 2021.
- [16] Fabian Isensee, Paul F Jaeger, Simon AA Kohl, Jens Petersen, and Klaus H Maier-Hein. nnu-net: a self-configuring method for deep learning-based biomedical image segmentation. *Nature methods*, 18(2):203–211, 2021.
- [17] Wonjae Kim, Bokyoung Son, and Ildoo Kim. Vilt: Vision-and-language transformer without convolution or region supervision. In *International conference on machine learning*, pages 5583–5594. PMLR, 2021.
- [18] Liunian Harold Li, Pengchuan Zhang, Haotian Zhang, Jianwei Yang, Chunyuan Li, Yiwu Zhong, Lijuan Wang, Lu Yuan, Lei Zhang, Jenq-Neng Hwang, et al. Grounded language-image pre-training. In *Proceedings of the IEEE/CVF Conference on Computer Vision and Pattern Recognition*, pages 10965–10975, 2022.
- [19] Yunxiang Li, Shuai Wang, Jun Wang, Guodong Zeng, Wenjun Liu, Qianni Zhang, Qun Jin, and Yaqi Wang. Gt u-net: A u-net like group transformer network for tooth root segmentation. In *Machine Learning in Medical Imaging: 12th International Workshop, MLMI 2021, Held in Conjunction with MICCAI 2021, Strasbourg, France, September 27, 2021, Proceedings 12*, pages 386–395. Springer, 2021.
- [20] Zihan Li, Yunxiang Li, Qingde Li, Puyang Wang, Dazhou Guo, Le Lu, Dakai Jin, You Zhang, and Qingqi Hong. Lvit: language meets vision transformer in medical image segmentation. *IEEE transactions on medical imaging*, 2023.
- [21] Ze Liu, Yutong Lin, Yue Cao, Han Hu, Yixuan Wei, Zheng Zhang, Stephen Lin, and Baining Guo. Swin transformer: Hierarchical vision transformer using shifted windows. In *Proceedings of the IEEE/CVF international conference on computer vision*, pages 10012–10022, 2021.
- [22] Jonathan Long, Evan Shelhamer, and Trevor Darrell. Fully convolutional networks for semantic segmentation. In *Proceedings of the IEEE conference on computer vision and pattern recognition*, pages 3431–3440, 2015.

- [23] Sergey P Morozov, Anna E Andreychenko, NA Pavlov, AV Vladzmyrskyy, NV Ledikhova, VA Gomboleviskiy, Ivan A Blokhin, PB Gelezhe, AV Gonchar, and V Yu Chernina. Mosmeddata: Chest ct scans with covid-19 related findings dataset. *arXiv preprint arXiv:2005.06465*, 2020.
- [24] Philip Müller, Georgios Kaissis, Congyu Zou, and Daniel Rueckert. Joint learning of localized representations from medical images and reports. In *European Conference on Computer Vision*, pages 685–701. Springer, 2022.
- [25] Ozan Oktay, Jo Schlemper, Loic Le Folgoc, Matthew Lee, Mattias Heinrich, Kazunari Misawa, Kensaku Mori, Steven McDonagh, Nils Y Hammerla, Bernhard Kainz, et al. Attention u-net: Learning where to look for the pancreas. *arXiv preprint arXiv:1804.03999*, 2018.
- [26] Shuyi Ouyang, Hongyi Wang, Shiao Xie, Ziwei Niu, Ruofeng Tong, Yen-Wei Chen, and Lanfen Lin. Slvit: Scale-wise language-guided vision transformer for referring image segmentation. In *Proceedings of the Thirty-Second International Joint Conference on Artificial Intelligence, IJCAI-23*, pages 1294–1302, 2023.
- [27] Ziyuan Qin, Huahui Yi, Qicheng Lao, and Kang Li. Medical image understanding with pretrained vision language models: A comprehensive study. *arXiv preprint arXiv:2209.15517*, 2022.
- [28] Alec Radford, Jong Wook Kim, Chris Hallacy, Aditya Ramesh, Gabriel Goh, Sandhini Agarwal, Girish Sastry, Amanda Askell, Pamela Mishkin, Jack Clark, et al. Learning transferable visual models from natural language supervision. In *International conference on machine learning*, pages 8748–8763. PMLR, 2021.
- [29] Olaf Ronneberger, Philipp Fischer, and Thomas Brox. U-net: Convolutional networks for biomedical image segmentation. In *Medical image computing and computer-assisted intervention—MICCAI 2015: 18th international conference, Munich, Germany, October 5-9, 2015, proceedings, part III 18*, pages 234–241. Springer, 2015.
- [30] Ashish Sinha and Jose Dolz. Multi-scale self-guided attention for medical image segmentation. *IEEE journal of biomedical and health informatics*, 25(1):121–130, 2020.
- [31] Nikhil Kumar Tomar, Debesh Jha, Ulas Bagci, and Sharib Ali. Tganet: Text-guided attention for improved polyp segmentation. In *International Conference on Medical Image Computing and Computer-Assisted Intervention*, pages 151–160. Springer, 2022.
- [32] Ashish Vaswani, Noam Shazeer, Niki Parmar, Jakob Uszkoreit, Llion Jones, Aidan N Gomez, Łukasz Kaiser, and Illia Polosukhin. Attention is all you need. *Advances in neural information processing systems*, 30, 2017.
- [33] Haonan Wang, Peng Cao, Jiaqi Wang, and Osmar R Zaiane. Uctransnet: rethinking the skip connections in u-net from a channel-wise perspective with transformer. In *Proceedings of the AAAI conference on artificial intelligence*, volume 36, pages 2441–2449, 2022.
- [34] Xue Wang, Zhanshan Li, Yongping Huang, and Yingying Jiao. Multimodal medical image segmentation using multi-scale context-aware network. *Neurocomputing*, 486:135–146, 2022.
- [35] Zhouxia Wang, Tianshui Chen, Guanbin Li, Ruijia Xu, and Liang Lin. Multi-label image recognition by recurrently discovering attentional regions. In *Proceedings of the IEEE international conference on computer vision*, pages 464–472, 2017.
- [36] Thomas Wolf, Lysandre Debut, Victor Sanh, Julien Chaumond, Clement Delangue, Anthony Moi, Pierric Cistac, Tim Rault, Rémi Louf, Morgan Funtowicz, et al. Transformers: State-of-the-art natural language processing. In *Proceedings of the 2020 conference on empirical methods in natural language processing: system demonstrations*, pages 38–45, 2020.
- [37] Enze Xie, Wenhai Wang, Zhiding Yu, Anima Anandkumar, Jose M Alvarez, and Ping Luo. Segformer: Simple and efficient design for semantic segmentation with transformers. *Advances in neural information processing systems*, 34:12077–12090, 2021.

- [38] Fei Xu, Lingli Lin, Zihan Li, Qingqi Hong, Kunhong Liu, Qingqiang Wu, Qingde Li, Yinhuan Zheng, and Jie Tian. Mrdff: A deep forest based framework for ct whole heart segmentation. *Methods*, 208:48–58, 2022.
- [39] Zhao Yang, Jiaqi Wang, Yansong Tang, Kai Chen, Hengshuang Zhao, and Philip HS Torr. Lavt: Language-aware vision transformer for referring image segmentation. In *Proceedings of the IEEE/CVF Conference on Computer Vision and Pattern Recognition*, pages 18155–18165, 2022.
- [40] Yuhao Zhang, Hang Jiang, Yasuhide Miura, Christopher D Manning, and Curtis P Langlotz. Contrastive learning of medical visual representations from paired images and text. In *Machine Learning for Healthcare Conference*, pages 2–25. PMLR, 2022.
- [41] Hengshuang Zhao, Jianping Shi, Xiaojuan Qi, Xiaogang Wang, and Jiaya Jia. Pyramid scene parsing network. In *Proceedings of the IEEE conference on computer vision and pattern recognition*, pages 2881–2890, 2017.
- [42] Jiawei Zhao, Yifan Zhao, and Jia Li. M3tr: Multi-modal multi-label recognition with transformer. In *Proceedings of the 29th ACM International Conference on Multimedia*, pages 469–477, 2021.
- [43] Zongwei Zhou, Md Mahfuzur Rahman Siddiquee, Nima Tajbakhsh, and Jianming Liang. Unet++: Redesigning skip connections to exploit multiscale features in image segmentation. *IEEE transactions on medical imaging*, 39(6):1856–1867, 2019.